Downregulation of Neurodevelopmental Gene Expression in iPSC-Derived Cerebral Organoids Upon Infection by Human Cytomegalovirus

Benjamin S. O'Brien[1], Rebekah L. Mokry[2], Megan L. Schumacher[2], Kirthi Pulakanti[3], Sridhar Rao[1,3], Scott S. Terhune[2], Allison D. Ebert[1]

1. Department of Cell Biology, Neurobiology, and Anatomy, Medical College of Wisconsin, Milwaukee, Wisconsin, United States

2. Department of Microbiology and Immunology, Medical College of Wisconsin, Milwaukee, Wisconsin, United States

3. Laboratory of Stem Cell Transcriptional Regulation, Blood Research Institute, Blood Center of Wisconsin, Milwaukee, United States

Corresponding author: aebert@mcw.edu

Keywords: Neural progenitor cells, RNAseq, cytomegalovirus, organoids, immediate early genes

Abstract

Human cytomegalovirus (HCMV) is a beta herpesvirus that, upon congenital infection, can cause severe birth defects including vision and hearing loss, microcephaly, and seizures. Currently, no approved treatment options exist for in utero infections. We previously demonstrated that HCMV infection decreases calcium signaling responses and alters neuronal differentiation in induced pluripotent stem cell (iPSC) derived neural progenitor cells (NPCs). Here we aimed to determine the impact of infection on the transcriptome in developing human neurons using iPSC-derived 3-dimensional cerebral organoids. We infected iPSC-derived cerebral organoids with HCMV encoding eGFP and sorted cell populations based on GFP signal strength. Significant transcriptional downregulation was observed including in key neurodevelopmental gene pathways in both the GFP (+) and intermediate groups. Interestingly, the GFP (-) group also showed downregulation of the same targets indicating a mismatch between GFP expression and viral infection. Using a modified HCMV virus destabilizing IE 1 and 2 proteins, we still observed significant downregulation of neurodevelopmental gene expression in infected neural progenitor cells. Together, these data indicate that IE viral proteins are not the main drivers of neurodevelopmental gene dysregulation in HCMV infected neural tissues suggesting therapeutically targeting IE gene expression is insufficient to restore neural differentiation and function.

Introduction

Human cytomegalovirus (HCMV) is a beta-herpesvirus with a 235-kbp double-stranded DNA (dsDNA) genome and the potential to express more than 700 proteins (Mocarski and Kemble 1996; Mocarski 2007). The virus infects a majority of the world's population with seroprevalence of 40-100% depending on age, socio-economic status and geographic location (Sinzger et al. 2008; Griffiths et al. 2015). Infection by HCMV is lifelong and can result in a range of conditions. Vertical transmission can also occur causing congenital CMV (cCMV) infection (Mocarski and Kemble 1996; Griffiths et al. 2015). A portion of babies born with cCMV infection will have long-term health problems including vision and hearing loss, microcephaly, and seizures. Neurological symptoms are likely the result of infection of neural progenitor cells (NPCs) (Luo et al. 2008; Hindley et al. 2012; Sun et al. 2020). In vitro, NPCs derived from both induced pluripotent stem cells (iPSCs) and fetal stem cells are fully permissive for HCMV infection, though susceptibility depends upon degree of NPC terminal differentiation (Odeberg et al. 2006; Luo et al. 2010; Pan et al. 2013; Gonzalez-Sanchez et al. 2015). In the fetal brain, NPCs are located in the bilateral subventricular zone aligned with the developing ventricle, and these cells express a number of key transcription factors that are required for maintenance of the progenitor cell pool and subsequent differentiation. NPCs can differentiate into the multiple neuronal and glial lineages found in the central nervous system (CNS). HCMV infection of NPCs has been shown to alter differentiation and function (Luo et al. 2010; Liu et al. 2017a; Wu et al. 2018; Brown et al. 2019). However, the mechanisms controlling this remain to be fully established.

Upon infection, the HCMV genes are expressed in three sequential steps known as immediate early (IE), early (E), and late (L). Viral IE gene expression can be detected within hours of infection and total viral replication occurs within approximately 96 hours post infection (hpi)

(Mocarski 2007; Marcinowski et al. 2012; Griffiths et al. 2015). In general, IE proteins are responsible for inhibiting intrinsic and innate host cell responses and initiating the transcription of viral early genes. Viral early genes then regulate host cell function to allow for viral genome replication and packaging (Griffiths et al. 2015; Xu et al. 2018). Late viral genes are expressed after viral DNA replication has begun and encode mostly structural proteins required for egress (Mocarski 2007; Perng et al. 2011; D'Aiuto et al. 2012; Tirosh et al. 2015). Following primary infection, the virus may remain lytic, replicating and activating the immune system, or enter a latent stage lacking replication and immune system activation (Griffiths et al. 2015). HCMV can replicate in differentiated cell types to varying degrees (Marcinowski et al. 2012; Pan et al. 2013; Gonzalez-Sanchez et al. 2015). In symptomatic children and adults, HCMV infection can be managed using (val)ganciclovir, cidofovir, and/or foscarnet, all of which inhibit viral DNA synthesis, or letermovir, which targets viral DNA packaging into nucleocapsids (Britt and Prichard 2018; Pass and Arav-Boger 2018; Altman et al. 2019; Steingruber and Marschall 2020). There is no FDA-approved therapy for treating expecting mothers, making vaccine development a major public health priority. Clinical trials are being conducted for use of valganciclovir in infants and children with confirmed symptomatic and asymptomatic cCMV infections.

Initial human microarray experiments using RNA isolated from HCMV-infected NPCs identified several downregulated neurodevelopmental genes such as NES, SOX2/4, and OLIG1 along with disruptions to differentiation (Luo et al. 2010; D'Aiuto et al. 2012). A subsequent mechanistic study in NPCs demonstrated the ability for viral protein IE1 to cause the loss of SOX2 expression through trapping of unphosphorylated STAT3 in the nucleus (Wu et al. 2018). Meanwhile, recent RNAseq studies conducted in HCMV-infected cerebral organoids support these findings identifying SOX2, OLIG1, ENO2, ALDOC, and FEZF2 among other downregulated

neurodevelopmental genes (Brown et al. 2019; Sun et al. 2020). These studies also found upregulation in ontology terms interleukin, inflammatory, and immune response with downregulation in ontology terms axonogenesis, calcium regulation, and glycolytic processes (Sun et al. 2020). Further, this work identifies the potential interaction of the PDGFRa receptor and viral pentameric complex in promoting virus entry into NPCs (Rak et al. 2018; Sun et al. 2020). It also found that administration of HCMV neutralizing antibody (NAbs) was sufficient to prevent infection and disruptions to structural development within the organoid (Sun et al. 2020). Additional work from us and others using the cerebral organoid model have found consistent disruptions to neuronal differentiation, cortical layering, calcium signaling, and electrical activity after HCMV infection (Brown et al. 2019; Sison et al. 2019; Sun et al. 2020).

In the current study we aim to identify neurodevelopmental transcriptional networks that are altered in response to HCMV infection and whether specific viral proteins contribute to gene misregulation. We found transcriptional downregulation among many genes which was not limited to cells expressing high levels of GFP, a surrogate marker of viral replication and was observed throughout the infected tissue. Previous studies have suggested that HCMV IE1 viral protein expression can regulate host gene expression (Marcinowski et al. 2012; Khan et al. 2014; Pignoloni et al. 2016; Liu et al. 2017b; Adamson and Nevels 2020). We found this to be the case for some gene targets, while regulation of others appeared to be independent of IE1/2 protein expression suggesting that other HCMV-related mechanisms are involved. Together, this work reveals that limiting IE gene expression offers minimal benefit on neural differentiation and function suggesting that therapeutic development against cCMV infection will require a more comprehensive approach.

Results

Cells from infected neural organoids exhibit reduced transcriptional profiles despite varying levels of viral gene expression.

Human iPSC-derived cerebral organoids were generated from two independent healthy control iPSC lines (Ebert et al. 2013; Sison et al. 2019) and infected after 30 days of development with a recombinant HCMV strain TB40/E expressing EGFP. Because tissues varied in size and likely cell numbers, we infected organoids using 500 infectious units per µg of tissue (IU/µg) and allowed infection to progress for two weeks. We detected GFP fluorescence by 4 days post infection (dpi), increased at 8 dpi, and continued to be present at 12 dpi indicating viral spread (Fig. 1A). At 14 dpi, HCMV-infected and mock-treated uninfected organoids (Fig. 1B) were dissociated into single cell suspensions, and cells were sorted based on levels of GFP fluorescence as an indirect measurement of infection (Fig. 1C). The gating parameters for live cells were set based on cells isolated from uninfected mock-treated organoids (Fig. S1). This approach is routinely used to investigate latency in HCMV-infected hematopoietic cells (Rak et al. 2018). The EGFP gene is present within the viral genome and expressed using an SV40 promoter, and fluorescence is postulated to be proportional to transcriptionally competent HCMV genomes (Rak et al. 2018; Collins-McMillen et al. 2019). We sorted cells into groups exhibiting high, intermediate, and undetectable levels of fluorescence (Fig. 1C). We defined these populations as GFP positive (+), GFP intermediate (Inter), and GFP negative (-). For example, the total number of live cells from a representative experiment was approximately 3.5 $x10^6$ which consisted of 0.5 $x10^6$ GFP (-) cells, 2 $x10^6$ GFP (Inter) cells, and $1x10^6$ GFP (+) cells (Fig. 1C). Infection did not cause large scale cell death as we observed that the number of live cells within each infected organoid group were comparable to the uninfected mock group (Fig. 1D). High expression of GFP

126 likely represents a population of cells exhibiting high viral genome copies and viral gene
127 expression. In contrast, cells isolated based on the absence of fluorescence are anticipated to be
128 uninfected, or perhaps newly infected with fluorescence below the threshold of detection. To
129 address these differences, we quantified levels of HCMV gene classes, immediate early (IE;
130 UL123, UL122), early-late (E-L; UL44) and late (L; UL99) with late expression dependent on
131 viral genome synthesis (Chambers et al. 1999). Cell populations of GFP (+) and GFP (Inter)
132 exhibited high levels of viral gene expression in all classes with differences consistent with their
133 levels of fluorescence (Fig. 1E). In the GFP (-) group, we did observe low but statistically
134 significant levels of viral IE RNAs (Fig.1E) likely representing a mixture of uninfected and newly
135 infected cells within the tissues.

136 We quantified infection-induced changes to host cell gene expression using RNA
137 sequencing on sorted cell populations from infected organoids and sorted cells isolated from
138 uninfected Mock-treated tissues. These studies were completed using three biological replicate
139 experiments that were sequenced separately with multiple organoids combined for each condition.
140 Mock and infected samples were mixed for each biological replicate resulting in the pooled library.
141 Samples had at least 2.5 million aligned reads and the External RNA Controls Consortium (ERCC)
142 spike-in was used to normalize variation in RNA expression across samples. After trimming, 80%
143 of the bases had a quality score of 30 indicating the probability of an incorrect base call was 1 in
144 1000. One of the GFP (+) replicates was removed from our subsequent analysis due to a large drop
145 off in total number of mapped reads likely related to technical error in the sequencing reaction.
146 Initially, we performed principal component analysis (PCA) on the data sets which revealed two
147 groups (Fig. 2A). One group contained the Mock-treated samples, and the other contained samples
148 isolated from infected organoids regardless of GFP signal strength (Fig. 2A). This was initially

surprising as we hypothesized that the subpopulations from infected organoids would cluster separately based on varying states of infection. However, as noted above, we did detect low levels of viral transcripts in the GFP (-) group indicating this population contains some infected cells. These data also suggest a possible indirect effect of HCMV on uninfected cells in the tissues.

We identified 1,222 cellular transcripts upregulated, 17,696 downregulated, and 2,882 not differentially expressed in GFP (+) cells from HCMV-infected tissues compared to cells from Mock tissues, using an adjusted p-value < 0.05 and 3-fold cutoff. In the GFP (-) population, we observed 911 transcripts upregulated and 18,379 downregulated compared to Mock. Table S1 and S2 contain full gene lists from DESEQ2 analysis along with a gene list of those not differentially expressed for GFP (+) vs Mock and GFP (-) vs Mock, respectively. Completion of hierarchical cluster analysis on the top 500 variable genes across samples showed distinct clustering between infected samples and mock samples (Fig. 2B, left), and we did not observe any additional clustering based on GFP designation following the removal of the mock data sets (Fig. 2B, right). These differences are shown in volcano plots for GFP (+) versus Mock and GFP (-) versus Mock (Fig. 2C) illustrating the disproportional number of genes being downregulated. For both GFP (+) and GFP (-) groups, over 90% of significantly differentially expressed genes were downregulated compared to cells isolated from uninfected Mock tissues. These observations demonstrate that HCMV infection profoundly impacts transcription of infected cells in neural tissues and supports a hypothesis that changes are occurring at very early times of infection (i.e., GFP (-) populations) and likely also involves indirect effects on uninfected cells from the neighboring GFP (+) infected cells.

Cell populations from HCMV-infected organoids display downregulation in critical neurodevelopmental and signaling genes.

To determine which biological processes are disproportionately altered in response to infection, we began by analyzing the complete data sets using Gene Set Enrichment Analysis (GSEA) that defines significant differences between two biological states in hallmark gene sets related to specific biological processes. Full gene lists for each analyzed gene set and rank metrics can be found in Supplemental Table 3. Compared to HCMV-infected GFP (+) cells, GSEA identified enrichment in genes up-regulated in response to alpha interferon proteins (Fig. 3A). We have included a representative heatmap of 40 genes out of the 97 hallmark genes in this category (Fig. 3A). This interferon response is known to occur during HCMV infection (Boyle et al. 1999; Paulus et al. 2006). Although GFP (+) and GFP (-) populations clustered together, this hallmark gene set was not significantly enriched in HCMV-infected GFP (-) compared to Mock (Fig. 3A). In contrast, HCMV-infected GFP (+) cells exhibited negative correlation and dysregulation in several sets (Fig.3B). This included genes up-regulated during the unfolded protein response, a subgroup of genes regulated by MYC, genes involved in the G2/M checkpoint, genes up-regulated in response to TGFß1, and genes up-regulated by activation of the PI3K/AKT/mTOR pathway. Disruption to genes involved with MYC, TGFß1, and AKT signaling in the GFP (+) population is likely related to infection causing an arrest in cell proliferation. We have included heatmaps of 40 genes within each hallmark set to further demonstrate that most genes were downregulated upon infection (Fig 3B). Our lab and others have demonstrated HCMV-mediated dysregulating of several of these processes in 2D cultures of primary human fibroblasts with many of the activities dysregulated by HCMV immediate early genes (Michelson et al. 1994; Jault et al. 1995; Kudchodkar et al. 2006; Moorman et al. 2008).

Next, we used gene ontology enrichment analysis to more precisely map specific processes that are impacted during infection. We analyzed the top 3,000 differentially expressed genes, both increased and decreased, between cells isolated from HCMV-infected GFP (+) and Mock-treated organoids. As noted earlier, most expression was downregulated in infected populations. Using a p-value cutoff of < 0.01, gene ontology (GO) analysis identified significant changes in 804 terms related to biological processes, 95 molecular functions, and 201 cellular components. The top five statistically significant terms are shown in Figure 5A with full lists in Table S5 and additional enriched terms in Figure S3 (additional ontology analysis performed using DAVID is found in Figure S3). The GO terms Ion Signaling, Cell-Cell Communication, and Junction Signaling were all significantly affected in HCMV GFP (+) cells (Fig. 4B). For example, we observed a 10.9-fold reduction in expression of GJA1, 7.8-fold reduction in CACNA1C, 5.7-fold reduction in CACNA1G, 5.4-fold for CAMKV, and 5.8-fold for KCNF1. We observed similar changes in the GFP (-) group compared to Mock, with GJA1 reduced by 11.2-fold, CACNA1C by 4.7-fold, CACNA1G by 5.6-fold and CAMKV by 7.1-fold (data not shown). KCNF1 was also downregulated but not significantly in the GFP (-) group. These data are consistent with previous studies demonstrating reduced expression of neuron-specific ion channel subunits and gap junctions (Luo et al. 2010; Khan et al. 2014) as well as our previous studies demonstrating reduced Ca^{2+} signaling in 2D NPC cultures and cells derived from HCMV-infected organoids (Sison et al. 2019).

We observed significant changes in the GO category Nervous System Development (Fig. 4B). In the GFP (+) cells compared to Mock, we quantified a 9.7-fold reduction in SOX2, 8.3-fold in FOXG1, 8.4-fold in DMRTA2, 7.8-fold in EMX1, and 9.5-fold in FEZF2. In GFP (-) cells, SOX2 decreased by 9.1-fold, FOXG1 by 7.5-fold, and FEZF2 by 8.5-fold while no significant

changes occurred in DMRTA and EMX. Numerous additional developmental genes that were significantly reduced in both GFP (+) and GFP (-) include HES1, PAX6, and NEUROG1 and G2 (Fig. 4B). The decrease in several of these transcription factors has been observations made in HCMV-infected NPCs (Luo et al. 2008; Luo et al. 2010; Li et al. 2015), and we have now expanded the observations to changes occurring within the context of a more complex 3D tissue model system.

The remaining most significantly enriched terms included cell cycle, cellular component organization, and RNA/protein binding (Fig. 5A) with several genes spanning multiple categories. Examples of genes related to cell cycle included NPM1 and PP2R1A, to cellular organization include NEFL and DPYSL2, and to RNA-protein binding include EEF2 and RPL3 (Fig. 4B). A complete list of GO terms enriched using the top 5,000 differentially expressed genes for GFP (+) and GFP (-) vs Mock as determined by adjusted p value of < 0.025 and fold change of > 5 are presented in Figure S3. We observed conservation of enriched terms between GFP (+) and GFP (-) populations including processes regulating protein expression, neuron differentiation, cellular component organization, and cell cycle.

Finally, we sought to define specific pathways using the Ingenuity Pathway Analysis tool. We analyzed the top 3,000 differentially expressed genes which defined 12 pathways as significantly altered during infection (Fig. 4C). Most pathway components are downregulated and consistent with results from the GO analysis. Several of these pathways involve regulating protein translation and degradation including protein ubiquitination, signaling relating to BAG2, EIF2 signaling, regulation of EIF4 and p70S6K, and mTOR signaling (Fig. S4A). Others related to neurodevelopmental processes such as Synaptogenesis Signaling Pathway and Huntington's Disease signaling (Fig. S4A). Meanwhile, RHOGDI signaling was one of a few pathways

containing several upregulated components and many of the unchanged genes between GFP (+) and Mock related to GPCR signaling (Fig. S4B). Finally, IPA's core analysis tool generated a node diagram connecting regulators from the major affected canonical pathways (Fig. S5). Several of these regulators fall into identified ontology classifications (TGFB1, RICTOR, NGF, and SP1) and have impacts on functional pathways that match our previous analyses. Complete analyses from IPA comparing GFP (+) vs Mock can be found in Supplemental Table S4.

Impact of HCMV replication on neurodevelopment gene expression.

The GFP (-) cell populations isolated from infected neural organoids exhibit profound changes in host transcriptomes. These GFP (-) cells exhibit low levels of HCMV IE gene expression, and (Wu et al. 2018) have demonstrated that expression of HCMV IE1 disrupts SOX2 expression in a STAT3-dependent mechanism (Reitsma et al. 2013). Therefore, we hypothesized that expression of viral proteins IE1 and possibly IE2 might be necessary to downregulate other key neurodevelopmental genes identified by our RNA seq experiments. To test their contributions, we infected cultures of NPCs using TB40r mGFP-IE-FKBP virus that expresses IE1 and IE2 with a destabilization domain (DD) tag in a shared exon (Glass et al. 2009). Addition of Shield1 ligand to the culture media prevents DD-dependent IE1 and IE2 degradation and increases its steady-state levels (Glass et al. 2009). We cultured neurosphere-derived NPCs for 3 and 7 days prior to infection to mimic developmental states. Cells were infected using TB40r mGFP-IE-FKBP at an MOI of 1.0 IU/cell, based on titers from fibroblasts, and we added 1 μM Shield1 ligand (Shield (+)) or vehicle (Shield (-)) starting at 2 hpi. We quantified changes in HCMV gene expression and observed significant reductions in IE RNAs UL123 (IE1) and UL122 (IE2) at all time points in Shield (-) compared to Shield (+) (Fig. 5A). Reductions in RNA levels for UL44 and UL99 also

occurred (Fig. 5B), and these differences were observed for infections done using Day 7 NPCs (Fig. 5A, B). We observed IE1-positive nuclei using immunofluorescence in Shield (+) but not Shield (-), albeit lower than the anticipated number of infected cells (Fig. 5C). Shield (+) IE1-positive cultures also exhibited reductions in TUJ1 and HES1, which is consistent with published studies (Liu et al. 2017b; Brown et al. 2019; Sun et al. 2020). Our data demonstrate that NPCs infected in the absence of Shield1 exhibit reduced HCMV IE1 protein and gene expression by 24 hpi as well as disruptions to additional viral gene classes.

We next asked whether destabilizing IE1 and IE2 in Shield (-) conditions could limit the downregulation of key developmental and transcription factors which we observed in GFP (+) and GFP (-) organoid populations. We infected NPCs as described above and measured differences in cellular gene expression of the nervous system developmental genes FEZF2, FOXG1, DMRTA1, and EMX1 in the Shield (+) and Shield (-) conditions (Fig. 6). We observed significant reductions in FEZF2 and FOXG1 RNA levels by 24 hpi in Day 3 NPCs, and by 48 hpi in Day 7 NPCs regardless of Shield1 (Fig. 6A). Changes in DMRTA2 and EMX1 occurred late during infection of Day 3 NPCs but was detectible by 24 hpi in Day 7 NPCs (Fig. 6B). There were some differences between Shield (+) and (-) conditions, but our data show that limiting IE1/IE2 protein expression was not sufficient to prevent the downregulation of any of the key neurodevelopmental targets explored. We next investigated a set of ion signaling, cell-cell communication and junctional organizational genes (Fig. 4B), specifically KCNF1, CACNA1C, CAMKV, CACNA1G, and GJA1 (Fig. 7). We consistently observed small decreases in calcium channel genes, KCNF1 and CACNA1C at late time points independent of Shield addition (Fig. 7A). Likewise, we observed decreases in CAMKV, CACNA1G, and GJA1. However, a Shield-dependent effect was noted particularly in the case of GJA1 and CAMKV (Fig. 7B,C). Together with our previous results

(Sison et al. 2019), our data confirm that HCMV mediated a disruption of several key neurodevelopmental and functional genes (Fig. 7D), but this effect has limited dependence on expression of IE1 and IE2.

Discussion

Stem cell-derived organoids provide a unique model system in which to study the developing human brain. For example, their 3D structure more closely represents the developing brain compared to 2D monolayer culture system and allows for the generation of a layered cortical structure expressing a wide variety of the markers associated with the human brain (Lancaster et al. 2013; Xu et al. 2018; Sison et al. 2019). We and others have previously demonstrated that cerebral organoids can be infected by HCMV with infection substantially altering organoid structure and function (Brown et al. 2019; Sison et al. 2019; Sun et al. 2020) (Figure 7D). However, a more thorough examination of how the transcriptional landscape is altered upon HCMV infection and what role viral proteins play in this process is needed to better understand the overall impact of HCMV infection on neural development.

Neurodevelopment is a highly complex process dependent on both spatial and temporal cues that activate large transcription factor networks within the NPC population. Ultimately, these cues cause NPCs to develop into a variety of terminally differentiated CNS cell types. RNA seq analysis of Day 30 organoids sorted for GFP signal strength as a proxy for the level of infection revealed downregulation of developmental transcription factors DMRTA2, FEZF2, EMX1, and FOXG1 in all populations regardless of GFP signal strength. These transcription factors are involved with the development of the telencephalon and regulation of early neuronal cell fate decision making. FEZF2 is typically expressed in the early cortical progenitor cell population and

is critical for fate specification of subcerebral projection neurons through activation of downstream transcription factor networks (Chen et al. 2008; Wang et al. 2011; Guo et al. 2013). FOXG1 knock-out mice experience severe microcephaly, a common phenotype of HCMV infection (Martynoga et al. 2005; Kumamoto and Hanashima 2017). In humans, FOXG1 syndrome, caused by mutations or deletions in the long (q) arm of chromosome 14, is characterized by impaired development and structural brain abnormalities (Tohyama et al. 2011; Chiola et al. 2019). DMRTA2 along with EMX1 are highly expressed in the developing dorsal telencephalon where research in mice reports reduced cortex size upon mutation (Shinozaki et al. 2004; Konno et al. 2012; Young et al. 2017). In addition to these roles, several of these transcription factors are involved in key signaling pathways with wide-ranging impacts. For example, DMRTA2 is cross regulated by the Wnt/β-catenin signaling pathway, FOXG1 is associated with the SHH pathway, and FEZF2 is an upstream regulator of cTIP2 and SATB2 regulating fate decisions (Chen et al. 2008; Kuwahara et al. 2010; Lui et al. 2011). Interestingly, despite no overt indication of active viral replication, the GFP (-) population exhibit similar transcriptional effects as the GFP (+) and intermediate populations. This suggests that viral infection has more widespread consequences that likely go beyond active viral replication. Although further studies are needed to elucidate the mechanisms underlying the global effect on the transcriptional profile, disruption of cell-cell communication processes, spread of viral proteins, or distribution of tegument proteins that disrupt cellular differentiation and function could be potential mechanisms.

Several members of the basic helix loop helix (bHLH) transcription factor family, including HES1, ASCL1, NEUROG1/2, OLIG 2, and N-MYC were also significantly downregulated across infected organoid groups. This family overlaps with DMRTA2 in protecting NPC maintenance and has additional roles in controlling the timing behind NPC proliferation and

differentiation (Young et al. 2017). Previous research also indicates cross regulation of bHLH factors by FEZF2 and DMRTA2 (Seo et al. 2007; Yang et al. 2012; Genin et al. 2014; Liu et al. 2017a; Dennis et al. 2019). Further, bHLH factors like HES1 have previously been identified as downregulated in NPCs following HCMV infection (Liu et al. 2017a; Liu et al. 2017b; Dennis et al. 2019). N-MYC regulates fating and division of intermediate neural progenitors, has influence on the expression of other family members through downstream cascades, and is cross regulated by SHH and Wnt (Kuwahara et al. 2010). The exact mechanism by which HCMV impacts bHLH factors is not fully elucidated, but studies indicate that HCMV proteins can act directly on genes to affect transcription or translation, and viral kinases can also function as pseudo kinases to impart post-translational modifications on host proteins and transcription factors (Mocarski 2007; Marcinowski et al. 2012; Steingruber and Marschall 2020). Specifically, the viral kinase UL97 can act as CDK1, which post-translationally modifies many of the bHLH factors altering their functionality (Gill et al. 2012). The wide-ranging functions within the bHLH family and their involvement within many common signaling cascades highlights the complexity of the potential avenues by which HCMV infection can affect neurodevelopmental pathways (Li et al. 2015).

It is well established that NPCs exhibit impaired signaling, differentiation, and even apoptosis following HCMV infection (Luo et al. 2010; Brown et al. 2019; Sison et al. 2019; Sun et al. 2020) (Figure 7C). NPCs are the cell type most permissive to infection (Luo et al. 2008) and found abundantly within cultured cerebral organoids. NPCs form early developmental structures and differentiate into a wide range of cell types in the human brain. Previous work has shown that IE1 traps unphosphorylated STAT3 in the nucleus and contributes to the reduction in SOX2 expression HCMV infected NPCs (Wu et al. 2018). However, little else is known about how HCMV downregulates key neurodevelopmental targets. Data from fibroblast cultures indicate the

ability of HCMV infection to transcriptionally regulate host genes as well as degrade their protein products (Cohen and Stern-Ginossar 2014; Khan et al. 2014). Further, overexpression of IE1 or 2 alone in healthy fibroblasts infected with mutated virus unable to transcribe either IE gene demonstrated rescue in gene targets previously downregulated by infection (Luo 2010, Khan 2013). Therefore, we used a conditional approach to assess the role of IE1/2 on additional neurodevelopmental gene expression. Initially, infections were conducted at 7 days post plate down; however, we observed a lack of viral protein replication and low expression of viral proteins (Figure S2). These results were not entirely unexpected as other groups have reported that NPC differentiation is inversely correlated to infectability (Odeberg et al. 2006; Gonzalez-Sanchez et al. 2015). While our experiments using the TB40r mGFP-IE-FKBP virus support this idea, our data also show that infection at 7 days post plate down still results in transcript level downregulation despite incomplete viral replication (Figure 4, S2). Although this downregulation was not as significant or sustained as what was observed in the 72-hour post plate down infection, these data indicate that viral material and/or partially replicating virus is capable of inducing acute transcriptional changes in more differentiated NPCs. The neurodevelopmental targets assessed following infection with the TB40r mGFP-IE-FKBP virus to control IE1/2 expression were clearly downregulated. However, the results indicate that transcriptional downregulation was largely independent of IE1/2 expression, which further highlights the ability of other viral components to impact transcription and translation in infected NPCs.

Previous studies from us and others have shown that HCMV infection disrupts calcium and potassium signaling in infected NPCs and organoids (Brown et al. 2019; Sison et al. 2019; Sun et al. 2020). We therefore hypothesized that these functional deficits could be due to downregulation of channel encoding genes responsible for ion transport and maintaining membrane potential.

Several such targets showed downregulation within the GFP (+) and intermediate groups (Fig. 3G). CACNA1C and CACNA1G are genes that encode unique voltage gated calcium channel subtypes. CACNA1G expression gives rise to T-type calcium channels that belong to the low voltage activated subgroup. Recently, mutations in CACNA1G have been shown to be associated with early onset cerebellar ataxia and epilepsy (Calhoun et al. 2016; Barresi et al. 2020). The gene CACNA1C encodes a critical subunit leading to the formation of L-type calcium channels. L-type channels have a prominent role in controlling gene expression through coupling membrane depolarization with cAMP response element-binding protein (CREB) phosphorylation via local Ca2+/calmodulin-dependent protein kinase II (CAMKII) signaling; interestingly, both CAMKIIB and Calmodulin 1/3 (CALM1/3) are downregulated following infection (Zhang et al. 2005; Liang et al. 2016) thus limiting the ability of CREB to act as the transcriptional regulator of nearly 4,000 downstream gene targets (Wheeler et al. 2012; Chiola et al. 2019). In mice it has been demonstrated that reduced expression of CACNA1C during development leads to a reduction in neurogenesis (Lee et al. 2016; Moon et al. 2018). This demonstrates that alterations to the expression of either CACNA1G or CACNA1C can cause phenotypes similar to those associated with congenital HCMV infection. CAMKV, while not involved in the activation of CREB, is a Ca^{2+}/calmodulin pseudo kinase that is required for the activity dependent maintenance of dendritic spines (Saneyoshi et al. 2010; Liang et al. 2016). It is unsurprising then that HCMV infected organoids and NPCs that display decreased neuronal firing and ability to transport calcium have CAMKV deficits as many of these processes are cross regulated (Odeberg et al. 2006; Brown et al. 2019; Sison et al. 2019; Sun et al. 2020). Meanwhile, several potassium channel encoding genes were downregulated in the GFP (+) and intermediate groups. These genes are important for potassium ion transport leading to neurotransmitter release and neural excitation. KCNF1, which

encodes a member of the voltage-gated potassium channel subfamily F, was particularly interesting because previous studies had shown it to be downregulated upon HCMV infection in NPCs (Luo et al. 2010; Young et al. 2011; Brown et al. 2019), and mutations in it and other family members have been linked to seizures and epilepsy, phenotypes of congenital HCMV infection (Kohling and Wolfart 2016).

Finally, GJA1, which encodes protein connexin-43, was downregulated in both GFP (+) and intermediate organoid groups compared to mock (Fig. 3,4). In addition to ion channels and calcium sensors, NPCs rely on gap and tight junctions to communicate with each other through intercellular ion transport (Wei et al. 2004; Goodenough and Paul 2009; Zhou and Jiang 2014). This type of communication can inform neural cell fating by cuing NPCs to continue proliferating or to begin differentiating (Lemcke and Kuznetsov 2013; Zhou and Jiang 2014). There is some evidence to suggest that HCMV hijacks the existing junctional machinery to spread viral material (Silva et al. 2005; Cohen and Stern-Ginossar 2014; Khan et al. 2014). In HCMV infected fibroblasts, there is clear evidence that expression of IE genes specifically leads to decreased expression of GJA1 and GJC1 (Luo et al. 2008; Khan et al. 2014). Intriguingly, our data suggest that this is also the case in NPCs (Fig. 6D). As such, we postulate that remodeling of the cell-cell communication network could be a way by which the virus impacts both signaling and development in the host and promotes cell-to-cell viral spread early in infection.

Despite the differences in viral strain, viral titre, and 2D vs 3D culture models, the shield (-) NPCs and isolated GFP (-) organoid cells have some interesting similarities. Previous studies show that the TB40r mGFP-IE-FKBP construct maintains a low level of viral transcript expression (Pan et al. 2016; Rak et al. 2018); however, our data suggest that this level of expression is likely not sufficient to cause full replication (Fig. 4, S2). Similarly, IE viral transcripts were still

significantly increased in the isolated GFP (-) cells compared to mock conditions despite a lack of robust GFP expression (Fig. 1D, 4). It is possible that if the GFP (-) cells were given more time in culture that GFP expression and E-L and L viral transcripts would be more evident. Nevertheless, significant downregulation of several gene targets was still observed in the absence of robust viral replication (Fig. 2,3,5,6) suggesting that the presence of some viral transcripts and/or viral material is sufficient to induce significant gene expression changes in neural tissues.

Taken together, we demonstrate that neurodevelopmental gene networks and critical neural signaling pathways are not dependent on IE1/2 protein expression indicating that other HCMV-related mechanisms are involved. Therefore, these data suggest that therapeutics designed to solely limit viral gene and protein expression may be insufficient to impact the widespread neural differentiation and functional deficits induced by congenital HCMV infection.

Materials and Methods

Cell culture and viruses

MRC-5 fibroblasts were cultured in Dulbecco's modified Eagle medium (DMEM) (ThermoFisher Scientific) containing 7% fetal bovine serum (FBS) (Atlanta Biologicals) and 1% penicillin-streptomycin (ThermoFisher Scientific). Cells were plated at 1.0×10^4 cells per well of a 24-well plate onto Matrigel coated coverslips. Matrigel was diluted in DMEM, placed on coverslips for approximately 12 hr, and aspirated off prior to plating cells. Virus stocks were prepared by infecting MRC-5 fibroblasts (ATCC) with HCMV strain TB40/E encoding EGFP (Umashankar et al. 2011). Cell culture medium was collected and pelleted through a sorbitol cushion (20% sorbitol, 50 mM Tris-HCl, pH 7.2, 1 mM $MgCl_2$) at 55,000 × g for 1 h in a Sorvall WX-90 ultracentrifuge and SureSpin 630 rotor (ThermoFisher Scientific). The TB40r mGFP-IE-

FKBP BAC was kindly provided by E. Borst (unpublished). The virus was cultured in the present of 1 µM Shield-1 (AOBIUS #AOB1848) and replaced every 24 hr. Titers of viral stocks were determined by a limited dilution assay with the 50% tissue culture infectious dose (TCID50) in MRC-5 cells in a 96-well dish. At 2 weeks post infection, HCMV IE1-positive cells were counted to determine viral titers, reported as the number of infectious units (IU) per milliliter. IE1-positive cells were determined using a mouse anti-HCMV IE1 antibody (clone 1B12; generously provided by Tom Shenk, Princeton University, Princeton, NJ).

Two independent iPSC lines were used (4.2 and 21.5/8) (Ebert et al. 2013). The iPSCs were grown and maintained in Essential 8 Media (ThermoFisher Scientific) and were cultured in feeder-free conditions on Matrigel (Corning). Neural progenitor cells (NPCs) were differentiated and maintained as neurospheres (EZ spheres) in Stemline (Millipore Sigma) supplemented with 0.5% N-2 supplement (ThermoFisher Scientific), 100 ng/ml EGF (Miltenyi Biotech), 100 ng/ml fibroblast growth factor (FGF; Stem Cell Technologies), and 5 ug/ml heparin (Millipore Sigma) as described previously (Ebert et al., 2013). Plated NPCs were grown in Neurobasal medium (ThermoFisher Scientific) supplemented with 2% B-27 (ThermoFisher Scientific) and 1% antibiotic-antimycotic (ThermoFisher Scientific). Cells were plated at 1.0×10^4 cells per well of a 24-well plate onto Matrigel coated coverslips. Matrigel was diluted in DMEM, placed on coverslips for approximately 12 hr, and aspirated off prior to plating cells.

Cerebral Organoids

Cerebral organoid cultures were differentiated from iPSCs according to the specification of the cerebral organoid kit from StemCell Technologies (#08570) that relies on an established protocol (Lancaster et al. 2013). These organoids were made from either of the two independent

WT stem cell lines (4.2 and 21.5/8), Infected 1 was derived from the 21.5/8 line, Infected 2 and 3 were derived from the 4.2 line, Mock 1 and 2 were derived from the 21.5/8 line, and Mock 3 and 4 were derived from the 4.2 line. (Ebert et al. 2013). Briefly, iPSCs were seeded at 9×10^3 cells per well onto 96-well ultralow attachment plates for embryoid body (EB) formation and grown in EB formation media (StemCell Technologies). At day 5, the induction of neural epithelium was initiated by moving the EBs into an ultralow attachment 24-well plate where they were then fed with induction media (StemCell Technologies). On day 7, neural tissues were embedded in Matrigel droplets and moved to ultralow attachment 6-well plates and fed expansion media (Stemcell Technologies). Then at day 10, the plate of developing organoids was transferred to a rocker which elicits the circulation of nutrients and prevents organoids from sticking to the dish. From this point on the organoids were fed maturation media (StemCell Technologies) every 3 days. At day 30, organoids were weighed and infected with 200-500 infectious units/ug HCMV strain TB40/E encoding GFP (Collins-McMillen et al. 2018; Rak et al. 2018; Collins-McMillen et al. 2019). Media was changed every 3-4 days. At 14 days post infection, organoids were either fixed for cryosectioning, prepped for FACs sorting, or dissociated in accutase enzyme and lysed for protein or RNA isolation. Three organoids containing approximately 1-2 million cells each were combined prior to sorting to ensure sufficient cell numbers in each population for whole transcriptome analysis.

FACs Sorting

Organoids were dissociated using the enzyme accutase at 37^{o}C for x min, and then washed in PBS. Organoid sorting buffer (1% FBS and 2 mM EDTA in DPBS) was then added to the tube and gently blown at the organoid until it completely dissociated. This cell suspension was then

493 filtered to remove any remaining cell clumps. Finally, the filtered suspension was placed on ice
494 until ready for sorting. Fluorescence Activated Cell Sorting (FACs) was performed on BD FACS
495 Diva 8.0.1. Live cell gating was established using the forward and side scatter plots from an
496 uninfected organoid. Infected organoids were then further sorted based on GFP fluorescence signal
497 into GFP (+), GFP intermediate, or GFP (-) that were consistent across replicates. Gating analysis
498 and plots were generated using Flowjo.
499
500 **RNA Sequencing and qRT-PCR**
501 Total RNA was isolated from organoid samples following FACs sorting for live cells and
502 GFP expression. To insure a high enough RNA concentration, 3 infected organoids were combined
503 for each N. After isolation RNA was analyzed on the tape station using screen tape from Agilent
504 (#5067-5576) for quantity and quality. External RNA Controls Consortium (ERCC) spike-in
505 control from Invitrogen (#4456740) was added to each sample to minimize external sources of
506 variability. cDNA libraries were then generated for each sample using the NEBNext Poly(A)
507 mRNA Magnetic Isolation Module (NEB #E7490). Libraries were then analyzed by qPCR
508 generating CT values using NEBNEXT Library Quant Kit (#E7630) and by tape station with
509 D1000 screen tape from Agilent (#5067-5582) to calculate fragment base pair size. These
510 measures were then analyzed by the NEB bio-calculator tool to get an estimated library
511 concentration. Libraries were then diluted to 4 nM and pooled. Another qPCR was run with the
512 pooled library to confirm concentration and a new dilution was performed if necessary. The diluted
513 pooled library (25 pM) was then combined with diluted NEXTSeq PhiX control (#FC-110-3002).
514 The PhiX control and library were then combined and loaded into the cartridge. Sequencing was

performed using the NextSeq 500/550 High Output Kit v2.5 (#20024906) from Illumina. Preliminary analysis was then performed using the online platform Basepair Technologies.

Total RNA was isolated, and reverse transcribed into cDNA using the Promega RT Kit (#A3500). q-RT-PCR was performed using specific primer sequences as outlined in (Table S5). The resulting CT values were normalized to GAPDH and the Delta Delta CT method was employed for analysis.

Immunofluorescence and Western Blot Analysis

Neural progenitor cells were fixed on coverslips with 4% paraformaldehyde (PFA) for 20 minutes at 4°C, washed with phosphate-buffered saline (PBS), and placed in PBS. For immunofluorescence, coverslips were blocked with 5% normal donkey serum (S30; Sigma) and 0.1% Triton in PBS for 30 min, incubated in primary antibodies overnight at 4°C, and incubated in secondary antibodies for 1 h at room temperature. The nuclear stain Hoechst was used to label nuclei. Primary antibodies used were HES1 (rabbit, PA5-28802; Thermo Fisher), UL123 (mouse;), and Tuj1 (chicken, GTX85469; GeneTex). Species-appropriate fluorescent secondary antibodies were used. An upright TS100 Nikon fluorescence microscope and NIS Elements were used for imaging and analysis.

Protein was isolated from NPCs or MRC5 fibroblasts by lifting the cells from the plate with trypsin (Invitrogen #15400-054) and lysing the cells in nuclear lysis buffer (10 mM NaCl, 50 mM Tris-HCl, pH 7.5, 1 mM EDTA, 1% SDS). Samples were then sonicated to ensure lyses and quantified using a Pierce BCA assay (ThermoFisher #23225). Equal amounts of protein (20 μg) were then loaded onto a 10% SDS-PAGE made with 2,2,2-trichloroethanol and run at 130 volts for 1 hour. Total protein was visualized via stain free detection on the Biorad ChemiDoc MP. Gels

were transferred to .45 μm Amershan Protran nitrocellulose membranes (Cytiva #10600002) using a BioRad Trans-Blot Turbo semi dry transfer system. Membranes were probed for IE1 (1:1000, clone 1B12, Shenk Lab), IE2 (1:1000, clone 3A9, Shenk Lab), UL44(1:10000, Virusys #CA006-100), and pp28 (1:1000 clone 10B4-29, Shenk Lab), using a goat α mouse HRP secondary (Jackson Immunoresearch Laboratories #115-035-003) detected by Novex ECL (Invitrogen #WP20005).

Data analysis

All statistical analysis was performed using Graph Pad Version 9. Data were collected from 3 independent organoid differentiations and infections and analyzed by one-way ANOVA or Student's T-test as appropriate with Tukey post hoc test for qPCR and western blot. $p<0.05$ was considered significant.

Bioinformatics

Fastq files were exported from Illumina sequence hub following sequencing then optical duplicates were removed and reference genome created using the raw fasta sequences for hg19. The raw RNA Seq reads are mapped and quantified to combined reference genome using Salmon v1.4.0. The read count matrix for all transcripts were utilized in R to make PCA plots and to run differential expression analysis. DESeq2 in R was used to perform the comparisons against mock samples to get significant up regulated and down regulated genes at adjusted P value < 0.05 and fold change of 3. Basepair Tech software and expression count analysis of the trimmed reads was conducted using STAR. Differentially expressed genes were identified by DESeq2 analysis using cutoffs of adjusted p-value <.05 and log2 fold change of ± 3. Gene ontology analysis was

subsequently performed using G-profiler and DAVID. Additional RNA seq analysis was performed using ingenuity pathway analysis from Qiagen and Gene Set Enrichment Analysis tool from UC San Diego and the Broad Institute. For both G-profiler and IPA analysis a list of the 3,000 most differentially expressed genes across samples analyzed were used. All these genes met the threshold of adj p-value < .01 and log2 fold change ± 9 as determined by DESeq2 analysis. For GSEA analysis the entire list of differentially expressed genes identified by DESeq2 meeting the adj p-value < .05 and log2 fold change of ± 3 cutoffs were used.

GSEA

Gene set enrichment analysis was performed using GSEA version 3.0 software with default parameters, classic enrichment, and phenotype permutations at 1000 times. GSEA was performed on differentially expressed genes determined from DESeq2 analysis of GFP (+) vs Mock and GFP (-) vs Mock samples using genes that met the cutoff of adj p-value of < .05 and log2 fold change ± 3. The enrichment plots displayed in Figure 3 were generated from analysis of GFP (+) vs Mock or GFP (-) vs Mock using the software's hallmark gene set

Acknowledgements

The authors would like to thank Tom Shenk for providing antibodies against HCMV proteins and Eva Borst for providing the TB40r mGFP-IE-FKBP virus. We thank Benedetta Bonacci in the Versiti-Blood Research Institute Flow Cytometry Core, and Emma Thomas for the artwork included in this work. Creation of this art is supported by the VI4-ArtLab Artist-in-Residence program. Finally, we thank members of the Terhune, Hudson, Rao, and Ebert laboratories for helpful discussions and input on the project.

584 Research reported in this publication was supported by the National Institute of Allergy
585 and Infectious Diseases division of the National Institutes of Health under award number
586 R01AI132414 (S.S.T. and A.D.E.) and R01CA2042031 (S.R.). The content is solely the
587 responsibility of the authors and does not necessarily represent the official views of the National
588 Institutes of Health.

589

590 All authors declare no conflicts of interests related to the manuscript. B.S.O, R.L.M, S.S.T.
591 and A.D.E. were responsible for study design. B.S.O., R.L.M., M.L.S., K.P., S.R. S.S.T., and
592 A.D.E. conducted experiments, analyzed data, and/or interpreted data. S.R., S.S.T., and A.D.E.
593 provided resources. B.S.O. R.L.M, and K.P. contributed to writing the manuscript. B.S.O, S.S.T.,
594 and A.D.E. wrote and edited the final manuscript.

595 **Figure Legends**

596 **Figure 1. Three-dimensional cerebral organoid infection with HCMV.** (A) On Day 30 of
597 differentiation, organoids were weighed and infected at 500 IU/ug with HCMV-TB40EGFP.
598 Bright-field and fluorescent images of one representative infected organoid taken at 4, 8, and 12
599 dpi are shown. (B) Images at 12 dpi of infected and uninfected organoids are displayed, one
600 representative organoid from each sorted group is shown. (C) Representative GFP intensity plot
601 from FACs analysis of an infected organoid and percentage of living cells in each organoid group
602 as determined by FACs each infected organoid group was made up of three pooled organoids. (D)
603 Percentage of live cells within whole infected and uninfected organoids across samples. (E) qPCR
604 analysis of viral gene expression within mock compared to GFP (+) and GFP intermediate
605 subpopulations. (F) qPCR analysis of viral gene expression within mock compared to the GFP (-)
606 subpopulation.

607

608 **Figure 2. All infected organoid subpopulations cluster distinctly from mock samples with**
609 **many genes being downregulated.** (A) PCA with components being all mapped genes across
610 samples split by axis determined by adj p-value and compared between each sample. (B)
611 Hierarchical cluster analysis of all sequenced samples for the top 500 most variable genes
612 according to read counts assigned. Hierarchical cluster analysis of only infected samples for the
613 top 500 most variable genes according to read counts assigned. (C) Volcano plot of the top 2,500
614 differentially expressed genes comparing GFP (-) vs. Mock as determined by adj p-value < .01.
615 Volcano plot of the top 2,500 differentially expressed genes comparing GFP (+) vs Mock as
616 determined by adj p-value. Arrows denote representative genes downregulated in both groups. (D)

617 Venn diagram comparing the 2,500 most differentially expressed genes in GFP (-) vs. Mock and
618 GFP (+) vs. Mock.
619
620 **Figure 3**. **Gene set enrichment analysis (GSEA) plots comparing infected organoid**
621 **populations to mock.** GSEA using the hallmark gene set on a list of all differentially expressed
622 genes with fold change ± 3 and adj p-value < .05. (A) Hallmark interferon alpha response
623 enrichment plots and corresponding heat maps from GFP (+) vs Mock and GFP (-) vs Mock
624 respectively. (B) Additional enrichment plots and heat maps (40 representative genes each) from
625 GSEA comparing GFP (+) vs Mock revealing significant de-enrichment in GFP (+) groups. A
626 normalized enrichment score (NES) and normalized p-value (NOM p-value) for each plot are
627 shown below, a cutoff of NOM p-value < .05 was used to establish significance.
628
629 **Figure 4. Pathway and ontology analysis conducted on GFP (+) vs Mock and heat maps**
630 **displaying up and downregulated genes.** (A) Gene Ontology analysis of the top 3,000
631 differentially expressed genes when comparing GFP (+) vs. Mock using fold change ± 3 and adj
632 p-value < .01. Terms listed were the five most significant across categories molecular function,
633 biological process, and cellular components. (B) Heat maps showing 20 representative genes
634 within the ontology classifications from (A), the values in the heat map are the average raw read
635 count number across GFP (+) or Mock samples. (C) Most significantly impacted canonical
636 pathways as determined by ingenuity pathway analysis using the same gene list as in (A). (D)
637 Node diagram generated from IPA core analysis using the same gene list as in (A) organized based
638 on most significantly affected canonical pathway regulators, how they interconnect and effect
639 downstream functions (Solid lines indicate direct interaction and dashed lines indicate indirect

640 interaction). (E) Heat maps containing 20 of the most significantly upregulated genes in GFP (+)
641 and GFP (-) groups vs Mock determined by adj p-value and fold change. For ontology and IPA
642 significance is displayed as -log(adj p-value) (Bolded genes within the heat maps identify those
643 used in subsequent shield-1 experiments).
644
645 **Figure 5. Infection of NPCs with TB40r mGFP-IE-FKBP virus results in limited expression**
646 **of viral proteins UL122/UL123 unless shield-1 is administered.** NPCs were infected at 3- or 7-
647 days post plate down with **TB40r mGFP-IE-FKBP** at an MOI of 1. One group was then
648 supplemented with 1 uM shield-1 daily (shield +) while the other was given vehicle (shield -). (A)
649 Immunofluorescent images at 24, 48, and 72 hpi from NPCs infected 3 days post plate down with
650 HCMV-IE1/IE2-ddFKBP and probed for HCMV IE gene IE1 (green), neuronal specific beta-
651 tubulin Tuj1 (purple), neurodevelopmental transcription factor Hes1 (red), Hoescht (blue), and
652 merge (All images taken at 20X, Using Nikon TL-1). (B-C) Expression of HCMV viral genes
653 (UL122 (IE), UL123 (IE), UL44 (E), and UL99 (L)) within NPCs infected 3- or 7- days post plate
654 down at 24, 48, and 72 hours post infection (hpi) as determined by qPCR. Stars were assigned
655 based on level of significance as determined by T-test: * = $p \leq .05$, ** = $p \leq .01$, *** = $p \leq .001$,
656 and **** = $p \leq .00001$.
657
658 **Figure 6. Neurodevelopmental gene targets are downregulated within NPCs infected with**
659 **TB40r mGFP-IE-FKBP independent of shield-1 administration.** (A-B) qPCRs were performed
660 for several key neurodevelopmental transcription factors (FezF2, FOXG1, DMRTA2, and EMX1)
661 within the HCMV-IE1/IE2-ddFKBP infected (shield +) and (shield –) groups plus uninfected
662 (mock) NPCs at both 3- and 7- days post plate down infected NPCs. No effect of shield

663 administration was observed for these targets. Stars were assigned based on level of significance
664 as determined by ANOVA: * = $p \leq .05$, ** = $p \leq .01$, *** = $p \leq .001$, and **** = $p \leq .00001$.
665
666 **Figure 7. Signaling and cell-cell communication gene targets are downregulated within NPCs**
667 **infected with TB40r mGFP-IE-FKBP depending on shield-1 administration.** Following the
668 same parameters as Figure 6, qPCRs were conducted for expression of signaling, cell-cell
669 communication, and junctional genes (CACNA1C, CACNA1G, CAMKV, KCNF1, and GJA1).
670 (A) For these targets shield administration had no impact on gene expression levels. (B,C) A shield
671 dependent effect was observed when comparing shield (-) and shield (+) infected groups for these
672 targets. Stars were assigned based on level of significance as determined by ANOVA: * = $p \leq .05$,
673 ** = $p \leq .01$, *** = $p \leq .001$, and **** = $p \leq .00001$. (D) Graphical summary integrating current
674 literature with this study's findings regarding HCMVs impact on development within NPCs and
675 cerebral organoids.
676
677 **Supplementary**
678 **Figure S1. Representative FACs traces from an HCMV-TB40EGFP infected organoid.** (A)
679 Set of three scatter analysis plots used to determine the live cell population within the organoid,
680 live cell gates were set based on the uninfected condition. (B) Table breaking down relative cell
681 counts within each gated population. (C) Plot of GFP signal intensity against total number of sorted
682 cells, GFP gates were set based on previous infected organoid sorting. (D) Relative number of
683 cells within each infected subpopulation, broken down by replicate.
684

Figure S2. Representative FACs traces from an uninfected organoid. (A) Set of three scatter analysis plots used to determine the live cell population within the organoid, live cell gates were set based on the uninfected condition. (B-C) Side scatter versus GFP plot in an uninfected organoid showing lack of GFP signal. (D) Percentage of live cells across all organoids sorted for sequencing.

Figure S3. Additional gene ontology analysis for GFP (+) vs. Mock and GFP (-) vs. Mock. (A) Ontology conducted using the same 3,000 gene list as in Figure 3A with the platform DAVID instead of G-profiler. Results shown are the top 20 most significant terms.

Figure S4. Network diagrams generated from IPA, summarize three key affected canonical pathways that were differentially affected by infection. (A) Synaptogenesis signaling pathway- log(adj p-value) = 16.367 majority of pathway components were downregulated. (B) mTOR signaling -log(adj p-value) = 17.479 majority of pathway components were downregulated. (C) RHOGDI signaling -log(adj p-value) = 11.123 mixture of upregulated and downregulated pathway components.

Figure S5. Ingenuity pathway core analysis diagram for GFP (+) vs. Mock. (A) Node diagram generated using IPA to connect major affected pathways and functional outcomes within the GFP (+) samples to regulators, done using the same gene list as IPA from Figure 3.

References

Adamson CS, Nevels MM. 2020. Bright and Early: Inhibiting Human Cytomegalovirus by Targeting Major Immediate-Early Gene Expression or Protein Function. *Viruses-Basel* **12**.

Altman AM, Mahmud J, Nikolovska-Coleska Z, Chan G. 2019. HCMV modulation of cellular PI3K/AKT/mTOR signaling: New opportunities for therapeutic intervention? *Antivir Res* **163**: 82-90.

Barresi S, Dentici ML, Manzoni F, Bellacchio E, Agolini E, Pizzi S, Ciolfi A, Tarnopolsky M, Brady L, Garone G et al. 2020. Infantile-Onset Syndromic Cerebellar Ataxia and CACNA1G Mutations. *Pediatr Neurol* **104**: 40-45.

Boyle KA, Pietropaolo RL, Compton T. 1999. Engagement of the cellular receptor for glycoprotein B of human cytomegalovirus activates the interferon-responsive pathway. *Mol Cell Biol* **19**: 3607-3613.

Britt WJ, Prichard MN. 2018. New therapies for human cytomegalovirus infections. *Antiviral Res* **159**: 153-174.

Brown RM, Rana P, Jaeger HK, O'Dowd JM, Balemba OB, Fortunato EA. 2019. Human Cytomegalovirus Compromises Development of Cerebral Organoids. *J Virol* **93**.

Calhoun JD, Hawkins NA, Zachwieja NJ, Kearney JA. 2016. Cacna1g is a genetic modifier of epilepsy caused by mutation of voltage-gated sodium channel Scn2a. *Epilepsia* **57**: E103-E107.

Chambers J, Angulo A, Amaratunga D, Guo H, Jiang Y, Wan JS, Bittner A, Frueh K, Jackson MR, Peterson PA et al. 1999. DNA microarrays of the complex human cytomegalovirus genome: profiling kinetic class with drug sensitivity of viral gene expression. *J Virol* **73**: 5757-5766.

Chen B, Wang SS, Hattox AM, Rayburn H, Nelson SB, McConnell SK. 2008. The Fezf2-Ctip2 genetic pathway regulates the fate choice of subcortical projection neurons in the developing cerebral cortex. *P Natl Acad Sci USA* **105**: 11382-11387.

Chiola S, Do MD, Centrone L, Mallamaci A. 2019. Foxg1 Overexpression in Neocortical Pyramids Stimulates Dendrite Elongation Via Hes1 and pCreb1 Upregulation. *Cerebral Cortex* **29**: 1006-1019.

Cohen Y, Stern-Ginossar N. 2014. Manipulation of host pathways by human cytomegalovirus: insights from genome-wide studies. *Semin Immunopathol* **36**: 651-658.

Collins-McMillen D, Buehler J, Peppenelli M, Goodrum F. 2018. Molecular Determinants and the Regulation of Human Cytomegalovirus Latency and Reactivation. *Viruses* **10**.

Collins-McMillen D, Rak M, Buehler JC, Igarashi-Hayes S, Kamil JP, Moorman NJ, Goodrum F. 2019. Alternative promoters drive human cytomegalovirus reactivation from latency. *Proc Natl Acad Sci U S A* **116**: 17492-17497.

D'Aiuto L, Di Maio R, Heath B, Raimondi G, Milosevic J, Watson AM, Bamne M, Parks WT, Yang L, Lin B et al. 2012. Human induced pluripotent stem cell-derived models to investigate human cytomegalovirus infection in neural cells. *PLoS One* **7**: e49700.

Dennis DJ, Han S, Schuurmans C. 2019. bHLH transcription factors in neural development, disease, and reprogramming. *Brain Res* **1705**: 48-65.

Ebert AD, Shelley BC, Hurley AM, Onorati M, Castiglioni V, Patitucci TN, Svendsen SP, Mattis VB, McGivern JV, Schwab AJ et al. 2013. EZ spheres: a stable and expandable culture system for the generation of pre-rosette multipotent stem cells from human ESCs and iPSCs. *Stem Cell Res* **10**: 417-427.

749 Genin EC, Caron N, Vandenbosch R, Nguyen L, Malgrange B. 2014. Concise Review: Forkhead
750 Pathway in the Control of Adult Neurogenesis. *Stem Cells* **32**: 1398-1407.
751 Gill RB, James SH, Prichard MN. 2012. Human cytomegalovirus UL97 kinase alters the
752 accumulation of CDK1. *J Gen Virol* **93**: 1743-1755.
753 Glass M, Busche A, Wagner K, Messerle M, Borst EM. 2009. Conditional and reversible
754 disruption of essential herpesvirus proteins. *Nat Methods* **6**: 577-579.
755 Gonzalez-Sanchez HM, Monsivais-Urenda A, Salazar-Aldrete CA, Hernandez-Salinas A, Noyola
756 DE, Jimenez-Capdeville ME, Martinez-Serrano A, Castillo CG. 2015. Effects of
757 cytomegalovirus infection in human neural precursor cells depend on their differentiation
758 state. *J Neurovirol* **21**: 346-357.
759 Goodenough DA, Paul DL. 2009. Gap junctions. *Cold Spring Harb Perspect Biol* **1**: a002576.
760 Griffiths P, Baraniak I, Reeves M. 2015. The pathogenesis of human cytomegalovirus. *J Pathol*
761 **235**: 288-297.
762 Guo C, Eckler MJ, McKenna WL, McKinsey GL, Rubenstein JLR, Chen B. 2013. Fezf2
763 Expression Identifies a Multipotent Progenitor for Neocortical Projection Neurons,
764 Astrocytes, and Oligodendrocytes. *Neuron* **80**: 1167-1174.
765 Hindley C, Ali F, McDowell G, Cheng K, Jones A, Guillemot F, Philpott A. 2012. Post-
766 translational modification of Ngn2 differentially affects transcription of distinct targets to
767 regulate the balance between progenitor maintenance and differentiation. *Development*
768 **139**: 1718-1723.
769 Jault FM, Jault JM, Ruchti F, Fortunato EA, Clark C, Corbeil J, Richman DD, Spector DH. 1995.
770 Cytomegalovirus infection induces high levels of cyclins, phosphorylated Rb, and p53,
771 leading to cell cycle arrest. *J Virol* **69**: 6697-6704.
772 Khan Z, Yaiw KC, Wilhelmi V, Lam H, Rahbar A, Stragliotto G, Soderberg-Naucler C. 2014.
773 Human cytomegalovirus immediate early proteins promote degradation of connexin 43 and
774 disrupt gap junction communication: implications for a role in gliomagenesis.
775 *Carcinogenesis* **35**: 145-154.
776 Kohling R, Wolfart J. 2016. Potassium Channels in Epilepsy. *Cold Spring Harb Perspect Med* **6**.
777 Konno D, Iwashita M, Satoh Y, Momiyama A, Abe T, Kiyonari H, Matsuzaki F. 2012. The
778 Mammalian DM Domain Transcription Factor Dmrta2 Is Required for Early Embryonic
779 Development of the Cerebral Cortex. *Plos One* **7**.
780 Kudchodkar SB, Yu Y, Maguire TG, Alwine JC. 2006. Human cytomegalovirus infection alters
781 the substrate specificities and rapamycin sensitivities of raptor- and rictor-containing
782 complexes. *Proc Natl Acad Sci U S A* **103**: 14182-14187.
783 Kumamoto T, Hanashima C. 2017. Evolutionary conservation and conversion of Foxg1 function
784 in brain development. *Dev Growth Differ* **59**: 258-269.
785 Kuwahara A, Hirabayashi Y, Knoepfler PS, Taketo MM, Sakai J, Kodama T, Gotoh Y. 2010. Wnt
786 signaling and its downstream target N-myc regulate basal progenitors in the developing
787 neocortex. *Development* **137**: 1035-1044.
788 Lancaster MA, Renner M, Martin CA, Wenzel D, Bicknell LS, Hurles ME, Homfray T, Penninger
789 JM, Jackson AP, Knoblich JA. 2013. Cerebral organoids model human brain development
790 and microcephaly. *Nature* **501**: 373-379.
791 Lee AS, De Jesus-Cortes H, Kabir ZD, Knobbe W, Orr M, Burgdorf C, Huntington P, McDaniel
792 L, Britt JK, Hoffmann F et al. 2016. The Neuropsychiatric Disease-Associated Gene
793 cacna1c Mediates Survival of Young Hippocampal Neurons. *Eneuro* **3**.

794 Lemcke H, Kuznetsov SA. 2013. Involvement of connexin43 in the EGF/EGFR signalling during
795 self-renewal and differentiation of neural progenitor cells. *Cell Signal* **25**: 2676-2684.
796 Li XJ, Liu XJ, Yang B, Fu YR, Zhao F, Shen ZZ, Miao LF, Rayner S, Chavanas S, Zhu H et al.
797 2015. Human Cytomegalovirus Infection Dysregulates the Localization and Stability of
798 NICD1 and Jag1 in Neural Progenitor Cells. *J Virol* **89**: 6792-6804.
799 Liang ZY, Zhan Y, Shen Y, Wong CCL, Yates JR, Plattner F, Lai KO, Ip NY. 2016. The
800 pseudokinase CaMKv is required for the activity-dependent maintenance of dendritic
801 spines. *Nat Commun* **7**.
802 Liu XJ, Jiang X, Huang SN, Sun JY, Zhao F, Zeng WB, Luo MH. 2017a. Human cytomegalovirus
803 infection dysregulates neural progenitor cell fate by disrupting Hes1 rhythm and down-
804 regulating its expression. *Virol Sin* **32**: 188-198.
805 Liu XJ, Yang B, Huang SN, Wu CC, Li XJ, Cheng S, Jiang X, Hu F, Ming YZ, Nevels M et al.
806 2017b. Human cytomegalovirus IE1 downregulates Hes1 in neural progenitor cells as a
807 potential E3 ubiquitin ligase. *Plos Pathog* **13**.
808 Lui JH, Hansen DV, Kriegstein AR. 2011. Development and evolution of the human neocortex.
809 *Cell* **146**: 18-36.
810 Luo MH, Hannemann H, Kulkarni AS, Schwartz PH, O'Dowd JM, Fortunato EA. 2010. Human
811 Cytomegalovirus Infection Causes Premature and Abnormal Differentiation of Human
812 Neural Progenitor Cells. *Journal of Virology* **84**: 3528-3541.
813 Luo MH, Schwartz PH, Fortunato EA. 2008. Neonatal Neural Progenitor Cells and Their Neuronal
814 and Glial Cell Derivatives Are Fully Permissive for Human Cytomegalovirus Infection.
815 *Journal of Virology* **82**: 9994-10007.
816 Marcinowski L, Lidschreiber M, Windhager L, Rieder M, Bosse JB, Radle B, Bonfert T, Gyory I,
817 de Graaf M, da Costa OP et al. 2012. Real-time Transcriptional Profiling of Cellular and
818 Viral Gene Expression during Lytic Cytomegalovirus Infection. *Plos Pathog* **8**.
819 Martynoga B, Morrison H, Price DJ, Mason JO. 2005. Foxg1 is required for specification of ventral
820 telencephalon and region-specific regulation of dorsal telencephalic precursor proliferation
821 and apoptosis. *Dev Biol* **283**: 113-127.
822 Michelson S, Alcami J, Kim SJ, Danielpour D, Bachelerie F, Picard L, Bessia C, Paya C, Virelizier
823 JL. 1994. Human cytomegalovirus infection induces transcription and secretion of
824 transforming growth factor beta 1. *J Virol* **68**: 5730-5737.
825 Mocarski ES. 2007. Betaherpes viral genes and their functions. *Human Herpesviruses: Biology,*
826 *Therapy, and Immunoprophylaxis*: 204-230.
827 Mocarski ES, Jr., Kemble GW. 1996. Recombinant cytomegaloviruses for study of replication and
828 pathogenesis. *Intervirology* **39**: 320-330.
829 Moon AL, Haan N, Wilkinson LS, Thomas KL, Hall J. 2018. CACNA1C: Association With
830 Psychiatric Disorders, Behavior, and Neurogenesis. *Schizophrenia Bull* **44**: 958-965.
831 Moorman NJ, Cristea IM, Terhune SS, Rout MP, Chait BT, Shenk T. 2008. Human
832 cytomegalovirus protein UL38 inhibits host cell stress responses by antagonizing the
833 tuberous sclerosis protein complex. *Cell Host Microbe* **3**: 253-262.
834 Odeberg J, Wolmer N, Falci S, Westgren M, Seiger A, Soderberg-Naucler C. 2006. Human
835 cytomegalovirus inhibits neuronal differentiation and induces apoptosis in human neural
836 precursor cells. *J Virol* **80**: 8929-8939.
837 Pan D, Xuan BQ, Sun YM, Huang SW, Xie MR, Bai YD, Xu WJ, Qian ZK. 2016. An intein-
838 mediated modulation of protein stability system and its application to study human
839 cytomegalovirus essential gene function. *Sci Rep-Uk* **6**.

Pan X, Li XJ, Liu XJ, Yuan H, Li JF, Duan YL, Ye HQ, Fu YR, Qiao GH, Wu CC et al. 2013. Later Passages of Neural Progenitor Cells from Neonatal Brain Are More Permissive for Human Cytomegalovirus Infection. *Journal of Virology* **87**: 10968-10979.

Pass RF, Arav-Boger R. 2018. Maternal and fetal cytomegalovirus infection: diagnosis, management, and prevention. *F1000Res* **7**: 255.

Paulus C, Krauss S, Nevels M. 2006. A human cytomegalovirus antagonist of type I IFN-dependent signal transducer and activator of transcription signaling. *Proc Natl Acad Sci U S A* **103**: 3840-3845.

Perng YC, Qian ZK, Fehr AR, Xuan BQ, Yu D. 2011. The Human Cytomegalovirus Gene UL79 Is Required for the Accumulation of Late Viral Transcripts. *Journal of Virology* **85**: 4841-4852.

Pignoloni B, Fionda C, Dell'Oste V, Luganini A, Cippitelli M, Zingoni A, Landolfo S, Gribaudo G, Santoni A, Cerboni C. 2016. Distinct Roles for Human Cytomegalovirus Immediate Early Proteins IE1 and IE2 in the Transcriptional Regulation of MICA and PVR/CD155 Expression. *J Immunol* **197**: 4066-4078.

Rak MA, Buehler J, Zeltzer S, Reitsma J, Molina B, Terhune S, Goodrum F. 2018. Human Cytomegalovirus UL135 Interacts with Host Adaptor Proteins To Regulate Epidermal Growth Factor Receptor and Reactivation from Latency. *J Virol* **92**.

Reitsma JM, Sato H, Nevels M, Terhune SS, Paulus C. 2013. Human cytomegalovirus IE1 protein disrupts interleukin-6 signaling by sequestering STAT3 in the nucleus. *J Virol* **87**: 10763-10776.

Saneyoshi T, Fortin DA, Soderling TR. 2010. Regulation of spine and synapse formation by activity-dependent intracellular signaling pathways. *Curr Opin Neurobiol* **20**: 108-115.

Seo S, Lim JW, Yellajoshyula D, Chang LW, Kroll KL. 2007. Neurogenin and NeuroD direct transcriptional targets and their regulatory enhancers. *Embo J* **26**: 5093-5108.

Shinozaki K, Yoshida M, Nakamura M, Aizawa S, Suda Y. 2004. Emx1 and Emx2 cooperate in initial phase of archipallium development. *Mech Dev* **121**: 475-489.

Silva MC, Schroer J, Shenk T. 2005. Human cytomegalovirus cell-to-cell spread in the absence of an essential assembly protein. *P Natl Acad Sci USA* **102**: 2081-2086.

Sinzger C, Digel M, Jahn G. 2008. Cytomegalovirus cell tropism. *Curr Top Microbiol Immunol* **325**: 63-83.

Sison SL, O'Brien BS, Johnson AJ, Seminary ER, Terhune SS, Ebert AD. 2019. Human Cytomegalovirus Disruption of Calcium Signaling in Neural Progenitor Cells and Organoids. *J Virol* **93**.

Steingruber M, Marschall M. 2020. The Cytomegalovirus Protein Kinase pUL97: Host Interactions, Regulatory Mechanisms and Antiviral Drug Targeting. *Microorganisms* **8**.

Sun GQ, Chiuppesi F, Chen XW, Wang C, Tian E, Nguyen J, Kha M, Trinh D, Zhang HN, Marchetto MC et al. 2020. Modeling Human Cytomegalovirus-Induced Microcephaly in Human iPSC-Derived Brain Organoids. *Cell Rep Med* **1**.

Tirosh O, Cohen Y, Shitrit A, Shani O, Le-Trilling VTK, Trilling M, Friedlander G, Tanenbaum M, Stern-Ginossar N. 2015. The Transcription and Translation Landscapes during Human Cytomegalovirus Infection Reveal Novel Host-Pathogen Interactions. *Plos Pathog* **11**.

Tohyama J, Yamamoto T, Hosoki K, Nagasaki K, Akasaka N, Ohashi T, Kobayashi Y, Saitoh S. 2011. West Syndrome Associated With Mosaic Duplication of FOXG1 in a Patient With Maternal Uniparental Disomy of Chromosome 14. *Am J Med Genet A* **155a**: 2584-2588.

Umashankar M, Petrucelli A, Cicchini L, Caposio P, Kreklywich CN, Rak M, Bughio F, Goldman DC, Hamlin KL, Nelson JA et al. 2011. A novel human cytomegalovirus locus modulates cell type-specific outcomes of infection. *Plos Pathog* **7**: e1002444.

Wang ZB, Boisvert E, Zhang X, Guo M, Fashoyin A, Du ZW, Zhang SC, Li XJ. 2011. Fezf2 regulates telencephalic precursor differentiation from mouse embryonic stem cells. *Cereb Cortex* **21**: 2177-2186.

Wei CJ, Xu X, Lo CW. 2004. Connexins and cell signaling in development and disease. *Annu Rev Cell Dev Biol* **20**: 811-838.

Wheeler DG, Groth RD, Ma H, Barrett CF, Owen SF, Safa P, Tsien RW. 2012. Ca(v)1 and Ca(v)2 Channels Engage Distinct Modes of Ca2+ Signaling to Control CREB-Dependent Gene Expression. *Cell* **149**: 1112-1124.

Wu CC, Jiang X, Wang XZ, Liu XJ, Li XJ, Yang B, Ye HQ, Harwardt T, Jiang M, Xia HM et al. 2018. Human Cytomegalovirus Immediate Early 1 Protein Causes Loss of SOX2 from Neural Progenitor Cells by Trapping Unphosphorylated STAT3 in the Nucleus. *J Virol* **92**.

Xu H, Jiao Y, Qin S, Zhao W, Chu Q, Wu K. 2018. Organoid technology in disease modelling, drug development, personalized treatment and regeneration medicine. *Exp Hematol Oncol* **7**: 30.

Yang N, Dong ZQ, Guo S. 2012. Fezf2 Regulates Multilineage Neuronal Differentiation through Activating Basic Helix-Loop-Helix and Homeodomain Genes in the Zebrafish Ventral Forebrain. *J Neurosci* **32**: 10940-10948.

Young A, Machacek DW, Dhara SK, Macleish PR, Benveniste M, Dodla MC, Sturkie CD, Stice SL. 2011. Ion channels and ionotropic receptors in human embryonic stem cell derived neural progenitors. *Neuroscience* **192**: 793-805.

Young FI, Keruzore M, Nan XS, Gennet N, Bellefroid EJ, Li M. 2017. The doublesex-related Dmrta2 safeguards neural progenitor maintenance involving transcriptional regulation of Hes1. *P Natl Acad Sci USA* **114**: E5599-E5607.

Zhang XM, Odom DT, Koo SH, Conkright MD, Canettieri G, Best J, Chen HM, Jenner R, Herbolsheimer E, Jacobsen E et al. 2005. Genome-wide analysis of cAMP-response element binding protein occupancy, phosphorylation, and target gene activation in human tissues. *P Natl Acad Sci USA* **102**: 4459-4464.

Zhou JZ, Jiang JX. 2014. Gap junction and hemichannel-independent actions of connexins on cell and tissue functions--an update. *FEBS Lett* **588**: 1186-1192.

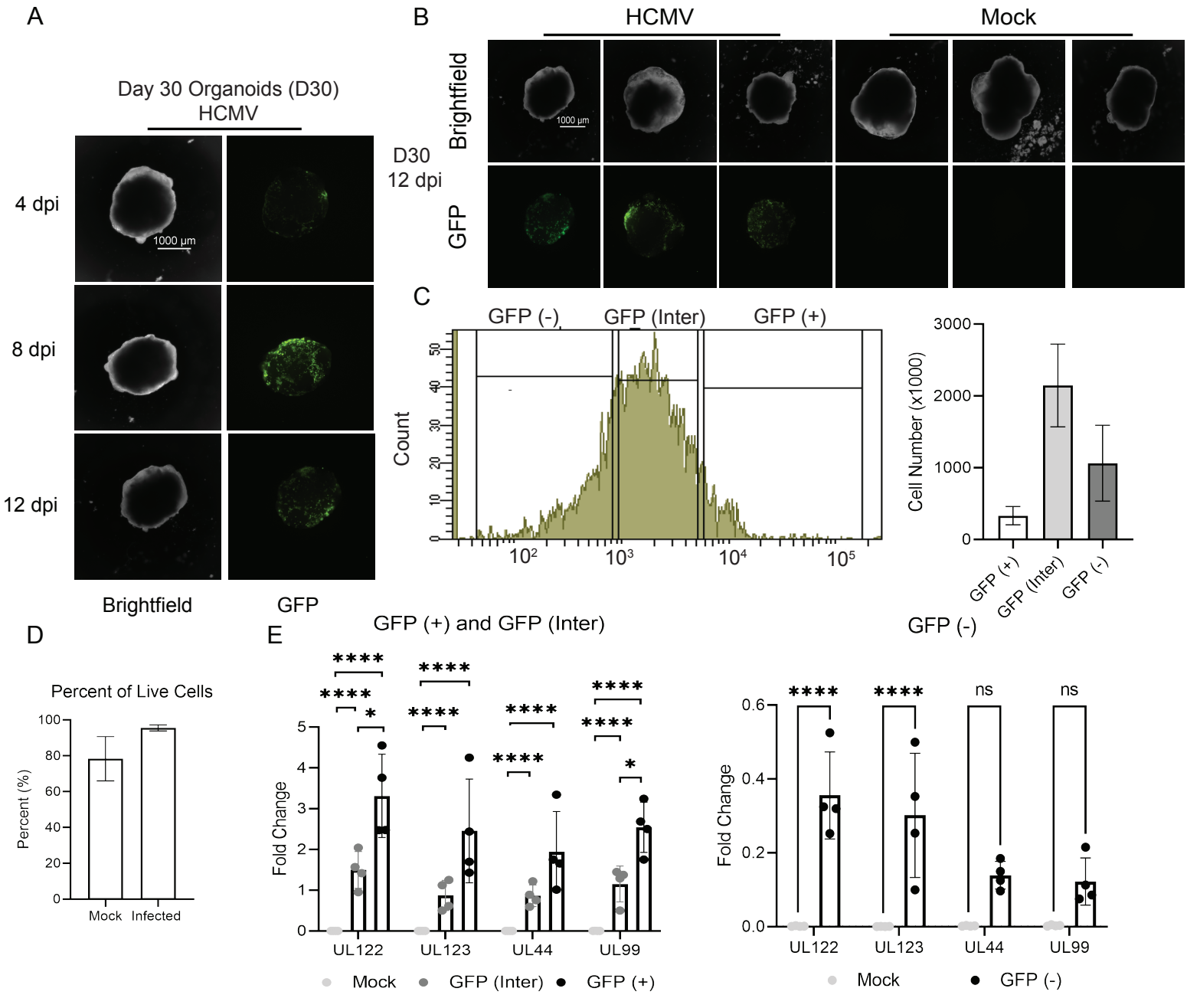

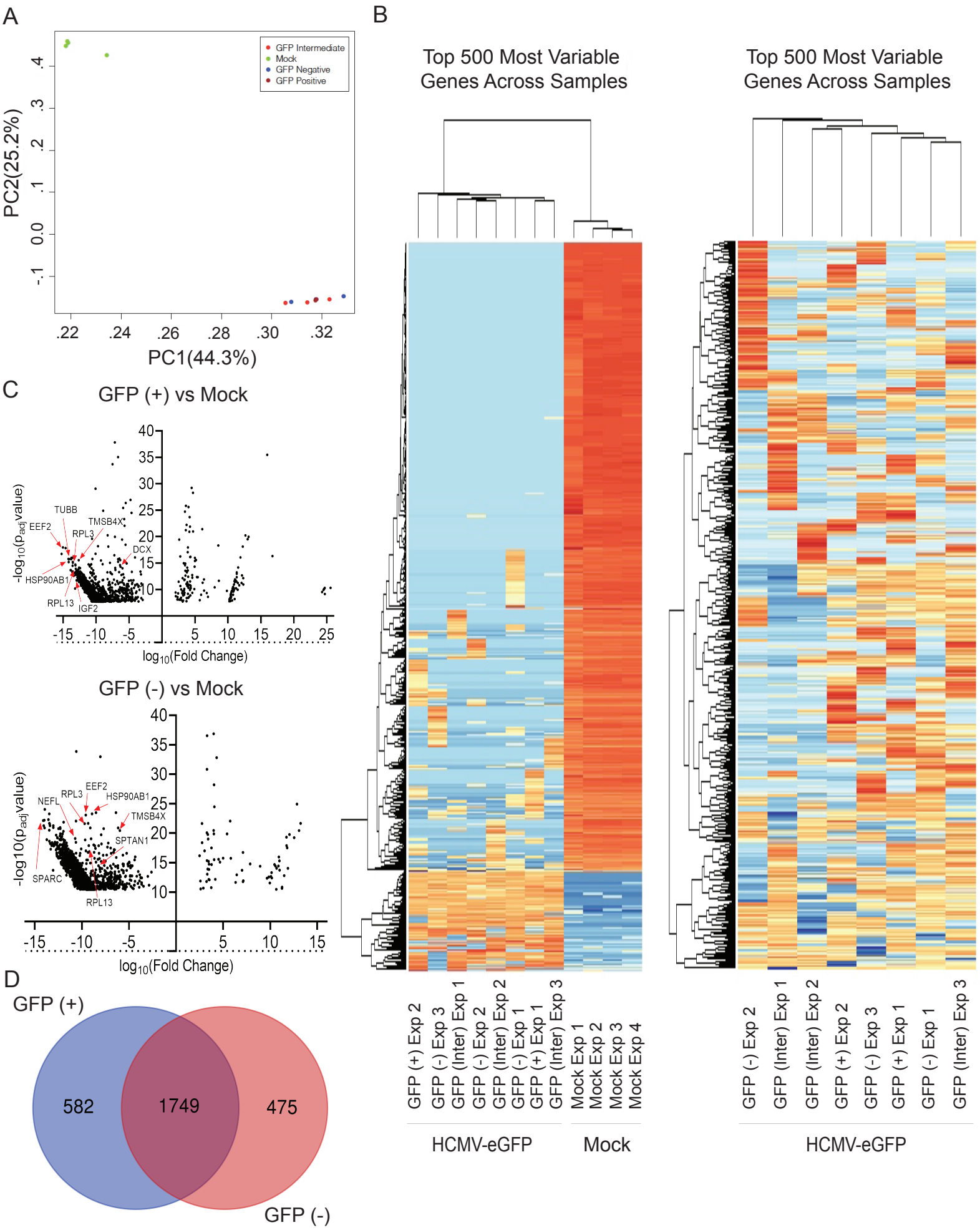

A

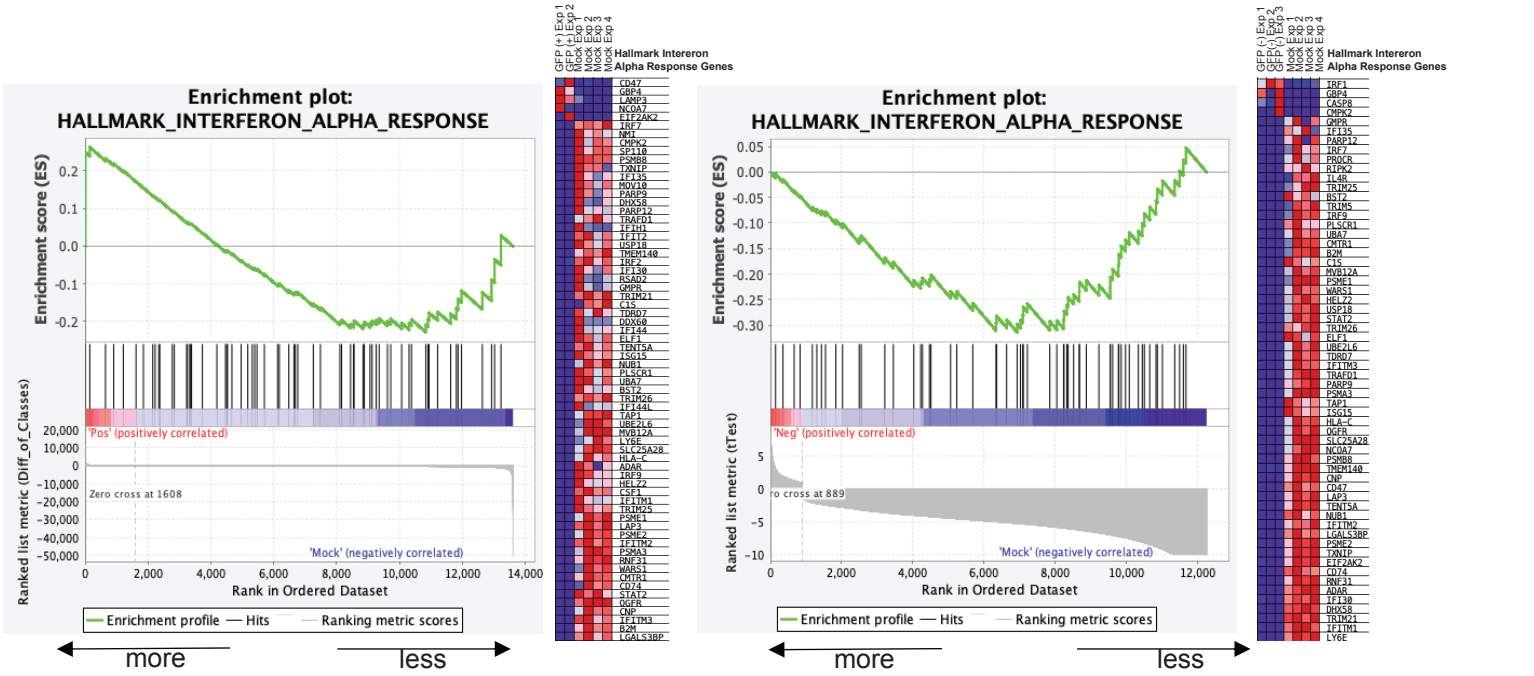

Levels of Enrichment in GFP (+) vs Mock
NES .64 NOM p-value .883

Levels of Enrichment in GFP (-) vs Mock
NES Not significant NOM p-value > 1

B

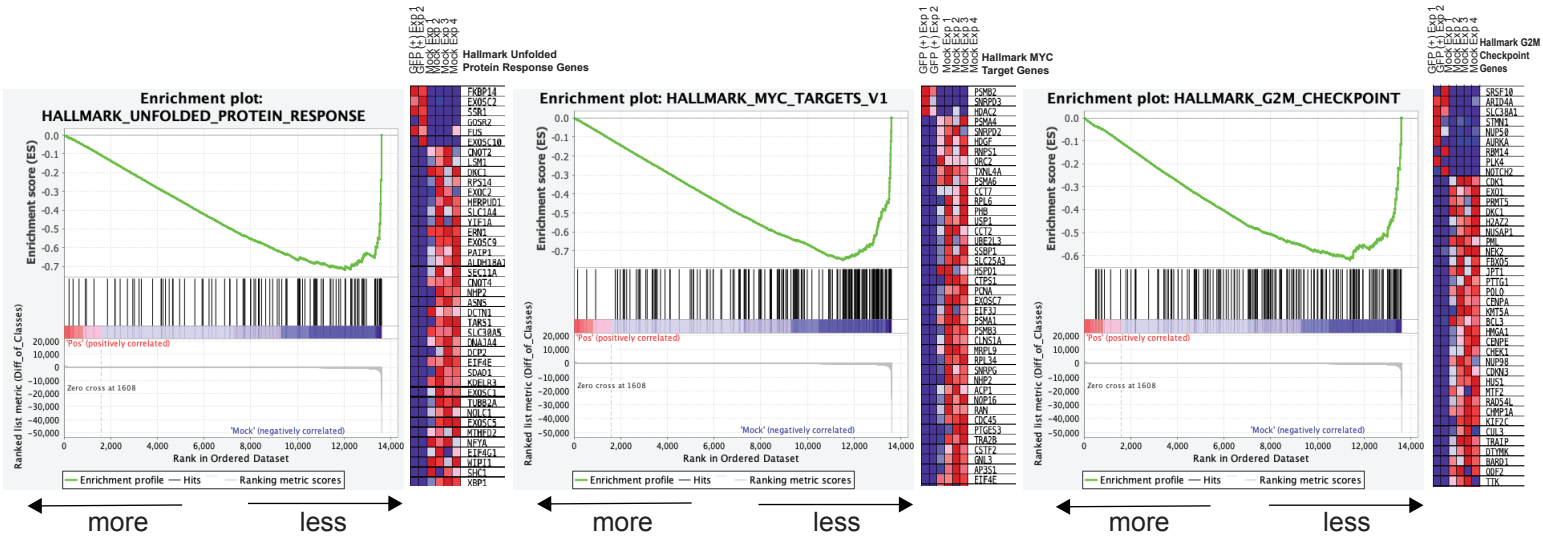

Levels of Enrichment in GFP (+) vs Mock
NES -1.37 NOM p-value < .01

NES -1.61 NOM p-value < .01

NES -1.17 NOM p-value < .2

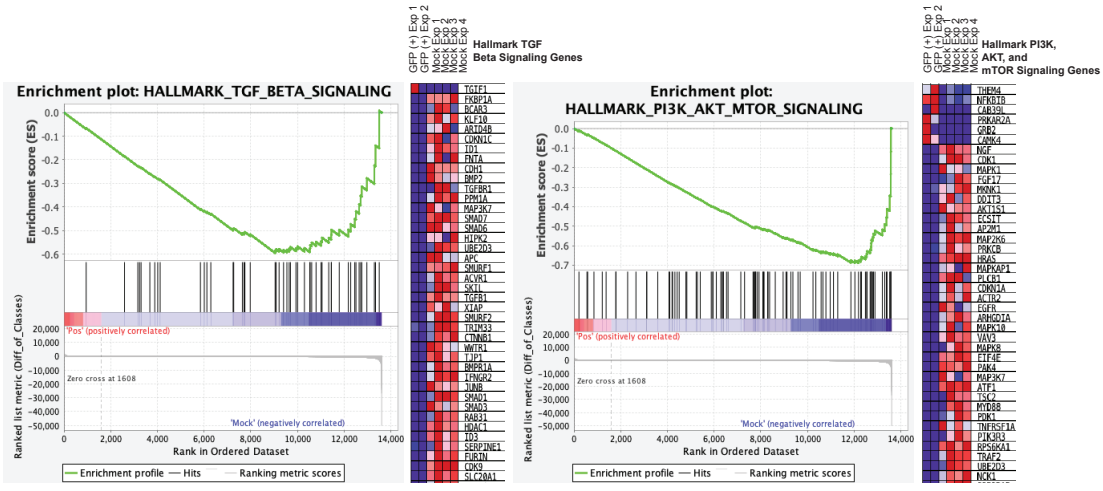

NES -1.31 NOM p-value < .01

NES -1.12 NOM p-value < .01

Figure 4

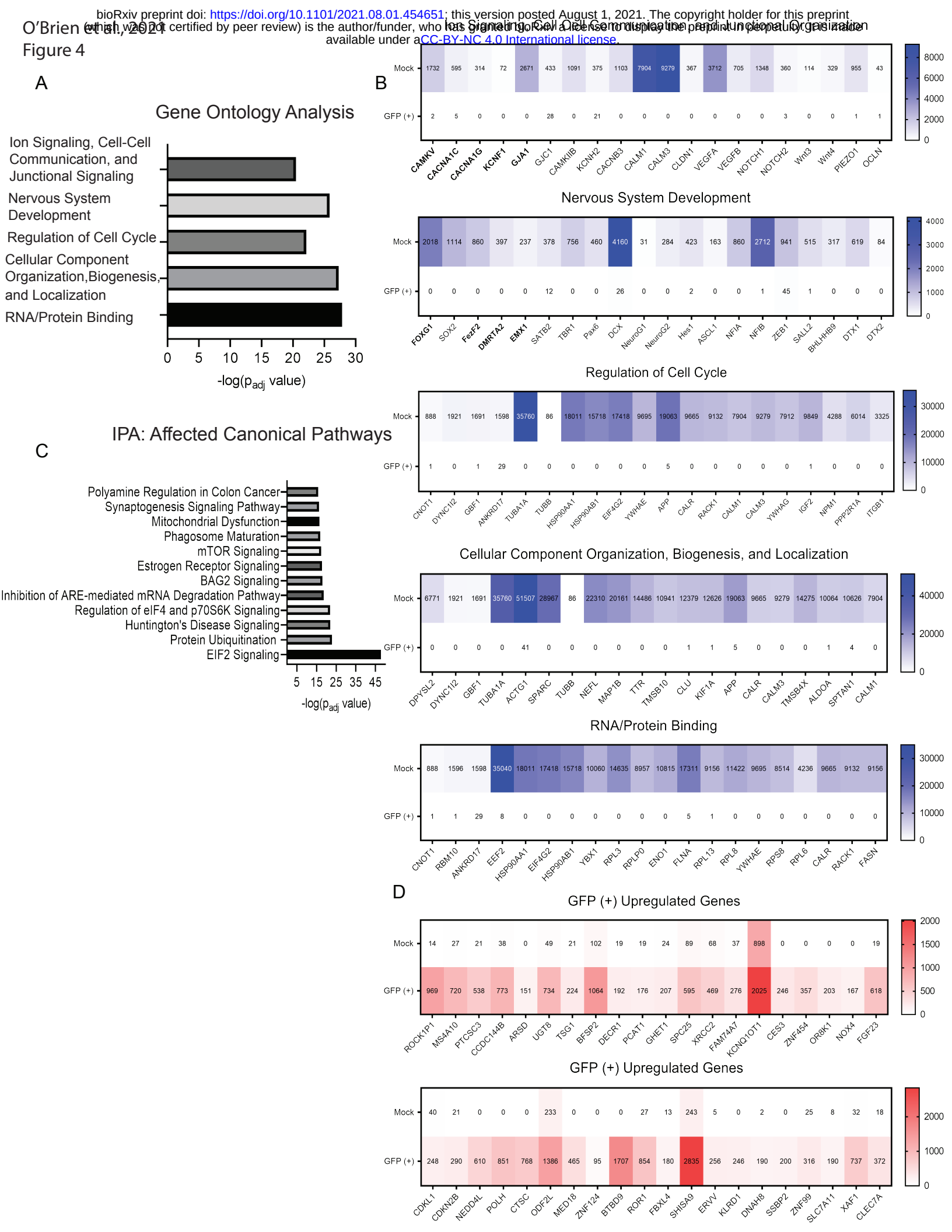

Figure 5

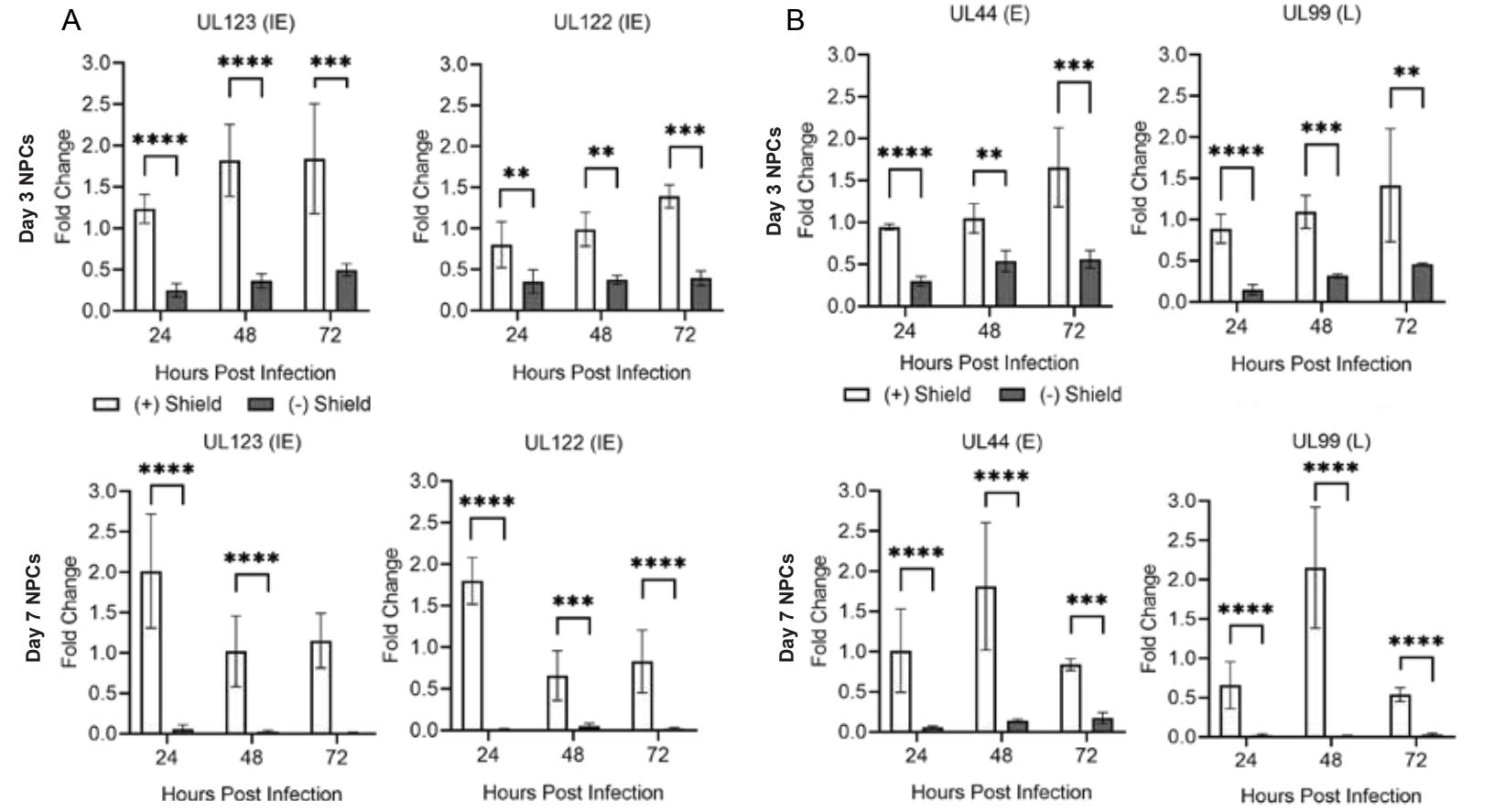

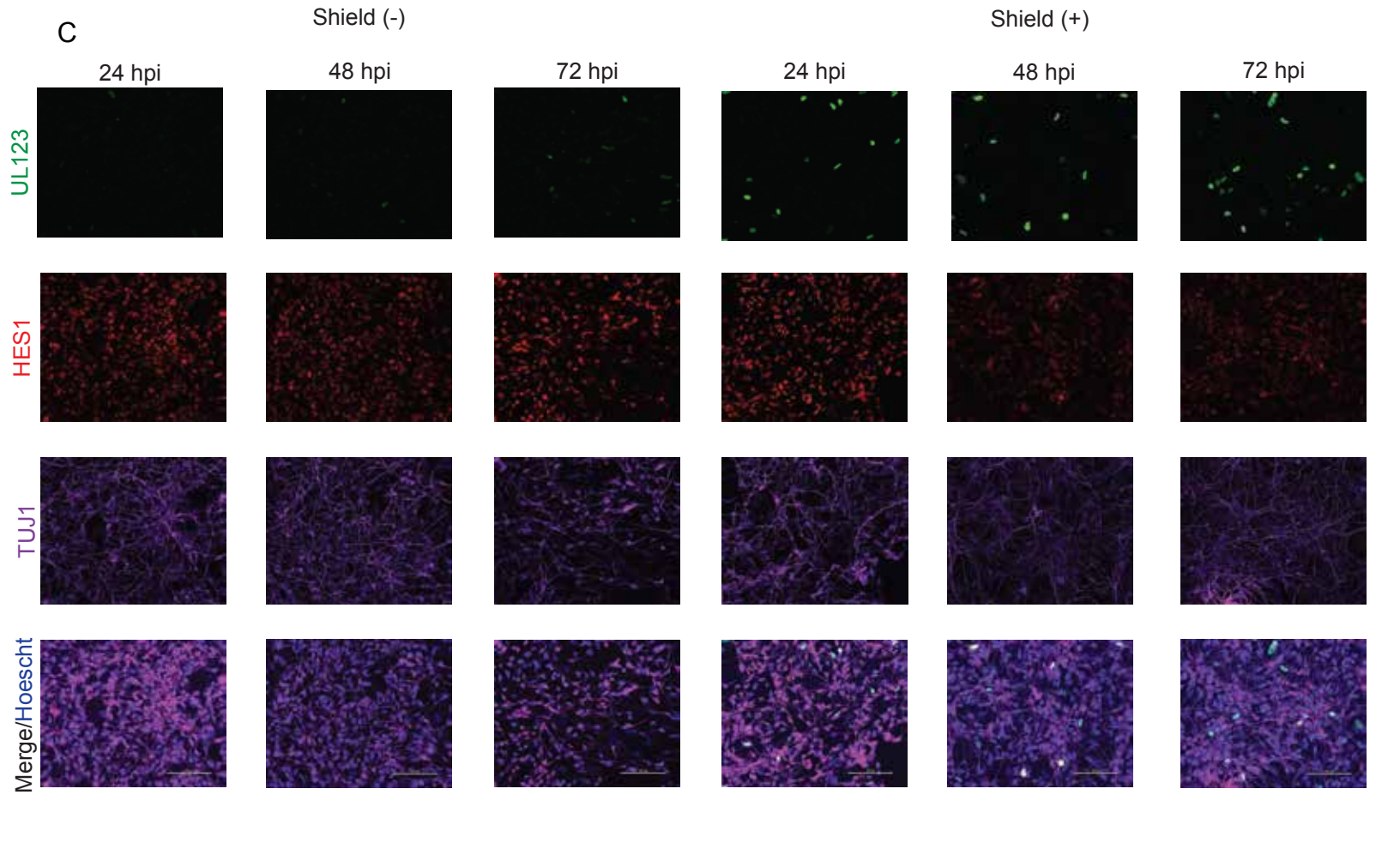

Figure 6